Pergamon

Geochimica et Cosmochimica Acta, Vol. 59, No. 13, pp. 2797–2815, 1995

0016-7037/95 $9.50 + .00

0016-7037(95)00174-3

An asteroidal breccia: The anatomy of a cluster IDP*

K. L. THOMAS,[1] G. E. BLANFORD,[2] S. J. CLEMETT,[3] G. J. FLYNN,[4] L. P. KELLER,[5] W. KLÖCK,[6] C. R. MAECHLING,[3] D. S. MCKAY,[7] S. MESSENGER,[8] A. O. NIER,[9] D. J. SCHLUTTER,[9] S. R. SUTTON,[10] J. L. WARREN,[1] and R. N. ZARE[3]

[1]Lockheed, 2400 Nasa Rd. 1, Houston, TX 77058, USA
[2]University of Houston-Clear Lake, Houston, TX 77058, USA
[3]Department of Chemistry, Stanford University, Stanford, CA 94305, USA
[4]Department of Physics, SUNY-Plattsburgh, Plattsburgh, NY 12901, USA
[5]MVA Inc., 5500/Suite 200 Oakbrook Pkwy., Norcross, GA 30093, USA
[6]Institute für Planetologie, Wilhelm-Klemm-Str. 10, 4400 Munster, Germany
[7]NASA/JSC, SN, Houston, TX 77058, USA
[8]McDonnell Center for the Space Sciences, Physics Department, Washington University, St. Louis, MO 63130, USA
[9]School of Physics and Astronomy, University of Minnesota, Minneapolis, MN 55455, USA
[10]Department of Geophysical Sciences, The University of Chicago, Chicago, IL 60637, USA

(*Received April* 22, 1994; *accepted in revised form March* 24, 1995)

Abstract—We report results of a consortium study of a large interplanetary dust particle known as cluster L2008#5. This cluster is composed of fifty-three fragments (>5 μm in diameter) and several hundred fines (<5 μm in diameter). Fragments and some fines were characterized using a variety of chemical and mineralogical techniques including: energy dispersive X-ray analyses for bulk chemical compositions for elements carbon through nickel, transmission electron microscopy for mineralogy, noble gas measurements, synchrotron X-ray fluorescence for trace element abundances, isotopic abundances using an ion probe, trace organic abundances, and reflectance spectroscopy. Our results show that cluster L2008#5 displays strong chemical and mineralogical heterogeneity on a size scale of the individual fragments (~10 μm in diameter). Despite the strong heterogeneity, we believe that nearly all of the analyzed fragments were originally part of the same cluster in space.

Several methods were used to estimate the degree of heating that this cluster experienced. Variations in the inferred peak temperatures experienced by different fragments suggest that a thermal gradient was maintained. The cluster as a whole was not strongly heated; it is estimated to have a low earth-encounter velocity which is consistent with origin from an object in an asteroidal orbit rather than from a comet, which would most likely have a high entry velocity.

Our conclusions show that cluster L2008#5 consists of a chemically and mineralogically diverse mixture of fragments. We believe that cluster L2008#5 represents a heterogeneous breccia and that it was most likely derived from an object in an asteroidal orbit. We also present an important cautionary note for attempts to interpret individual, small-sized 10–15 μm IDPs as representative of parent bodies. It is not unique that individual building blocks of IDPs, such as discrete olivine, pyroxene, sulfide grains, regions of carbonaceous material, and other noncrystalline material, are found in several fragments; however, it is unique that these building blocks are combined in various proportions in related IDPs from one large cluster particle.

INTRODUCTION

Since May of 1981, NASA at the Johnson Space Center (JSC) has used high-flying aircraft to collect interplanetary dust particles (IDPs) in the Earth's stratosphere. The conventional flat plates used for particle collection have a surface area of ~30 cm^2 and capture IDPs, typically with diameters ranging from ~2–25 μm. Within the past five years, large area collectors (LACs), with a tenfold increase in surface area, have also been used to sample the stratospheric particle population. The LACs were found to collect a greater number of larger sized extraterrestrial particles, many with diameters > 25 μm. Although some of these large IDPs remain intact when removed from the collectors, many collide with the collection surface, fracture, and produce fragments of various sizes. We used the term cluster particle for a fragmented, large IDP. In general, a cluster particle is a group of fragments in a clump on a collection surface with a minimum of three large-size fragments (>10 μm in diameter) and many fines (fragments < 5 μm in diameter). The study of cluster particles has several advantages over that of small-sized individual IDPs: (1) cluster IDPs provide a large amount of extraterrestrial material which may be relatively pristine or unheated, (2) fragments from the same cluster can be examined using a variety of techniques, and (3) cluster particles bridge the size-gap from conventional stratospheric IDPs to larger particles. These larger particles, or micrometeorites, generally range from ~100–1000 μm in diameter with a mass distribution peaking near 200 μm (Love and Brownlee, 1993). Extraterrestrial particles in this size range are, by mass, the most abundant material striking the Earth (Grün et al., 1985).

A preliminary mineralogical and chemical study of two to three fragments from several cluster particles showed that, in general, bulk compositions for most major elements were chondritic (within ~2 × CI), with the exception of carbon (Thomas

* This paper is dedicated to the memory of A. O. Nier who greatly contributed to the study of interplanetary dust particles.

Table 1
Bulk compositions of 53 fragments from cluster L2008#5 obtained by quantitative energy dispersive X-ray spectroscopy (EDX).

Fragment	Clu11	Clu13	Clu14	Clu15	Clu16	Clu17	Clu18	Clu19	Clu110	Clu111
Size*	9	15x25	10x20	10	20	10	8x10	10x10	10	12x12
C	14	3	2	2	4	12	4	14	10	6
Na	2.1	0.4	3.1	0.8	1.8	1.7	2.4	1.0	1.6	0.6
Mg	13.3	20.6	6.3	15.6	9.4	11.0	12.2	8.5	9.6	2.7
Al	0.8	0.6	3.1	1.6	1.7	1.2	1.2	1.0	0.9	0.3
Si	10.1	27.7	12.7	22.4	12.4	14.4	14.4	23.8	20.6	6.8
P	0.4	0.0	0.4	0.3	0.4	0.5	0.7	0.7	0.3	0.4
S	4.3	0.2	1.7	0.4	11.2	6.8	4.3	5.6	4.1	25.3
K	0.1	0.7	0.3	1.8	0.0	0.1	0.0	0.0	0.2	0.0
Ca	9.8	0.4	1.6	0.0	1.9	0.8	0.9	0.5	1.0	0.0
Ti	0.0	0.0	0.0	0.0	0.0	0.0	0.0	0.0	0.0	0.0
Cr	0.1	0.5	0.1	0.3	0.1	0.1	0.2	0.1	0.4	0.0
Mn	0.2	0.3	0.1	0.3	0.1	0.1	0.2	0.0	0.2	0.0
Fe	7.9	2.7	28.2	12.7	25.4	16.6	24.2	10.8	19.4	36.9
Ni	0.6	0.0	0.9	0.1	1.6	1.2	0.6	0.6	1.2	3.5
O	36.7	42.6	39.8	41.9	30.1	33.8	34.8	33.2	30.0	17.6
Total**	100.0	99.7	100.3	100.2	100.1	100.3	100.1	99.8	99.5	100.1

Fragment	Clu112	Clu113	Glu114	Glu115	Glu116	Glu117	Glu118	Glu119	Glu120	Glu1121
Size*	10x12	8x10	7x10	8x10	7x10	5x7	8x12	5x5	9x12	10
C	2	7	6	4	2	1	8	6	2	2
Na	1.5	1.0	0.9	1.2	2.2	1.6	0.9	1.6	0.9	1.0
Mg	1.3	17.6	11.3	11.6	9.7	5.1	5.0	8.3	20.4	18.7
Al	0.4	0.7	0.7	1.2	0.9	0.6	1.8	1.0	0.7	0.4
Si	5.6	22.7	11.0	15.4	12.4	10.3	21.5	11.8	26.4	22.3
P	0.4	0.4	0.4	0.3	0.5	0.3	0.4	0.5	0.3	0.2
S	3.9	2.8	13.2	6.7	5.2	7.8	0.5	13.5	0.5	0.2
K	0.0	0.0	0.0	0.0	0.1	0.3	0.3	0.0	0.0	0.0
Ca	0.1	0.2	0.6	1.1	0.9	0.4	13.8	0.6	0.3	0.0
Ti	0.0	0.0	0.0	0.0	0.0	0.0	3.6	0.0	0.0	0.0
Cr	0.9	0.1	0.2	0.2	0.3	0.5	0.0	0.0	0.2	0.3
Mn	0.0	0.1	0.4	0.3	0.3	0.1	0.0	0.1	0.0	0.3
Fe	51.8	6.4	26.8	23.2	30.8	37.6	1.3	25.2	3.5	13.7
Ni	3.4	0.3	1.2	1.3	1.0	2.5	0.0	1.5	0.0	0.0
O	28.2	40.9	27.1	33.5	33.2	31.5	43.0	30.2	44.1	41.2
Total**	99.5	100.2	99.8	100.0	99.5	99.6	100.1	100.3	99.3	100.3

Fragment	Clu21	Clu22	Clu23	Clu24	Clu25	Clu26	Clu27	Clu28
Size*	10x15	8x8	6x9	5x7	5x7	5x5	5x7	5x10
C	4	2	7	5	7	5	8	9
Na	3.2	0.1	1.9	2.7	2.3	1.9	2.6	2.6
Mg	4.4	0.5	9.7	11.8	11.7	11.0	9.1	10.5
Al	0.6	0.1	1.4	1.7	1.5	1.9	4.2	1.4
Si	7.9	0.9	13.3	14.5	15.3	18.4	12.8	14.0
P	0.5	0.2	0.6	0.9	0.6	0.4	0.8	0.6
S	7.1	23.4	9.4	2.8	5.4	6.2	2.0	4.1
K	0.1	0.0	0.1	0.0	0.1	0.3	0.2	0.1
Ca	0.2	0.0	0.5	0.9	0.9	0.1	0.8	0.9
Ti	0.0	0.0	0.0	0.0	0.0	0.0	0.0	0.0
Cr	0.1	0.0	0.3	0.2	0.2	0.2	0.1	0.2
Mn	1.0	0.1	0.1	0.3	0.2	0.1	0.1	0.2
Fe	38.1	57.6	23.4	17.6	18.4	18.8	19.4	19.0
Ni	4.0	0.2	1.5	0.8	1.1	1.8	1.1	1.3
O	29.1	15.2	31.0	40.3	35.6	33.8	39.3	36.3
Total**	100.2	100.4	100.2	99.5	100.3	99.9	100.5	100.2

et al., 1993a). However, the results also indicated that fragments from cluster particles can show chemical and mineralogical heterogeneities at the 10 μm scale which suggests that conclusions drawn from one fragment of a cluster are not necessarily representative of other fragments from the same cluster. These initial results prompted us to do a more systematic investigation of many fragments from one individual cluster particle. Here we report the results of a consortium study in which multiple fragments from one large cluster were distributed to several research groups and analyzed using a variety of mineralogical and chemical techniques. The main objectives of this study were (1) to determine if fragments from a single cluster are chemically and mineralogically heterogeneous, (2) to determine if heterogeneities extend to other properties of cluster IDPs, (3) to compare the chemical and mineralogical properties of a cluster IDP to chondrites, and (4) to compare reflectance spectra of a characterized cluster IDP to those of plausible parent bodies (e.g., asteroids and comets).

METHODS

We were allocated ~95% of the fragments from cluster particle #5 from the large area collector L2008. This cluster contained a mixture of optically light and dark fragments and subfragments, or fines, as observed in reflected light. Based on the number and size of the fragments, without considering pore spaces between individual fragments, we estimate that the original size of this cluster was ~40–50 μm in diameter. It is possible that the cluster is much larger if the porosity is higher (see section "What is the source of cluster

TABLE 1. (Continued)

Fragment	Clu31	Clu32	Clu33	Clu34	Clu35	Clu36	Clu37	Clu38	Clu39	Clu310
Size*	5x5	5x7	5x5	15x17	12x10	8x20	15x15	12x12	12x12	8x10
C	9	17	23	3	2	3	3	3	3	29
Na	2.2	2.4	2.0	0.4	3.0	1.7	1.0	0.5	4.5	1.5
Mg	10.4	8.7	7.1	3.6	9.0	9.6	8.8	2.7	7.0	8.1
Al	1.5	1.1	1.0	0.2	0.8	1.1	0.8	0.2	4.9	1.0
Si	16.4	16.4	16.4	5.8	11.3	12.2	13.1	3.0	19.2	12.3
P	0.5	0.5	0.5	0.2	1.2	0.7	0.1	0.3	3.7	0.5
S	3.4	4.5	6.6	12.4	1.5	9.2	1.0	25.6	1.2	5.9
K	0.1	0.1	0.1	0.0	0.1	0.0	0.0	0.0	0.7	0.1
Ca	1.0	0.6	0.6	0.2	0.7	1.0	1.0	0.0	13.3	0.5
Ti	0.0	0.0	0.0	0.0	0.0	0.0	0.1	0.0	0.0	0.0
Cr	0.2	0.1	0.1	0.2	0.2	0.2	0.3	0.0	0.4	0.1
Mn	0.1	0.1	0.1	0.1	0.4	0.2	0.3	0.0	0.1	0.1
Fe	15.7	13.8	11.6	46.0	34.5	25.5	38.4	47.8	3.7	10.5
Ni	0.7	0.7	0.6	3.0	0.9	2.6	1.8	0.5	0.2	0.6
O	38.5	34.0	30.3	25.0	34.2	32.9	30.2	16.2	37.8	29.8
Total**	100.0	99.9	100.0	100.1	99.8	99.9	99.9	99.8	99.7	99.9

Fragment	Clu311	Clu312	Clu313	Clu314	Clu315	Clu317	Clu318	Clu319	Clu320
Size*	10x10	8x8	8x8	5x12	9	8x10	7x10	8x8	10
C	4	9	15	14	15	2	4	4	12
Na	1.6	1.6	2.2	2.6	2.7	4.5	5.7	1.5	5.4
Mg	7.8	9.0	9.3	9.6	15.5	10.0	7.0	11.1	2.2
Al	0.7	1.4	1.3	1.4	0.9	3.9	10.6	1.2	0.5
Si	10.9	17.5	16.3	14.6	7.4	20.9	13.7	15.1	30.0
P	0.3	0.4	0.5	0.6	0.6	0.3	2.5	0.8	0.5
S	8.2	6.0	4.6	3.7	6.2	0.6	2.4	6.6	0.3
K	0.1	0.1	0.0	0.0	0.0	0.2	0.1	0.0	0.5
Ca	0.8	0.4	0.6	0.6	0.5	0.2	4.0	1.0	0.1
Ti	0.0	0.0	0.0	0.0	0.0	0.0	0.0	0.0	0.0
Cr	0.3	0.2	0.1	0.1	0.0	0.0	0.1	0.3	0.0
Mn	0.2	0.1	0.1	0.0	0.1	0.3	0.1	0.2	0.4
Fe	33.5	18.6	12.5	15.8	12.1	17.9	8.6	20.3	0.9
Ni	1.9	1.1	0.7	0.8	0.3	0.1	0.5	1.2	0.0
O	29.9	34.4	37.1	36.1	38.9	39.4	40.9	36.4	47.1
Total**	100.2	99.8	100.2	99.9	99.9	100.3	100.2	99.7	99.9

Fragment	Clu51	Clu52	Clu53	Clu54	Clu55	Clu56
Size*	10x7	6x6	7x7	10x10	10x10	5x8
C	4	13	5	12	4	4
Na	2.3	1.6	1.8	1.3	2.3	1.3
Mg	9.2	9.6	10.2	10.2	9.4	11.7
Al	0.8	2.0	1.0	1.0	1.8	1.2
Si	13.3	18.3	15.7	16.5	16.0	17.4
P	0.6	0.7	0.6	0.5	0.5	0.6
S	10.6	5.0	7.0	9.4	5.8	9.4
K	0.0	0.1	0.0	0.0	0.0	0.0
Ca	1.0	2.2	0.9	0.8	0.5	0.9
Ti	0.0	0.0	0.0	0.0	0.0	0.0
Cr	0.1	0.1	0.3	0.2	0.1	0.3
Mn	0.1	1.0	0.2	0.2	0.2	0.2
Fe	23.1	11.3	26.1	17.1	19.4	16.4
Ni	2.3	0.6	1.2	0.8	4.3	0.9
O	32.3	35.1	29.9	30.5	36.1	35.3
Total**	99.7	100.6	99.9	100.5	100.4	99.6

*Size in micrometers
**Totals may not equal 100.0; C abundances are reported as whole number values

L2008#5?"). Fragments include three that are ~15 × 15 μm, six that are ~12 × 12 μm, ~50 that range from 5–10 μm in diameter, and several hundred subfragments (also called fines) < 5 μm in diameter. The fifty-three fragments (>5 μm in diameter) from cluster L2008#5 were placed on beryllium substrates for analysis at JSC using a JEOL 35 CF scanning electron microscope (SEM) operated at 15 kV and equipped with a Princeton Gamma Tech (PGT) X-ray energy dispersive (EDX) spectrometer. The PGT spectrometer is a detector with a thin organic window which was used to determine bulk particle compositions; this spectrometer allows detection of elements with $Z > 5$. Our complete procedures and analytical checks for quantitative SEM EDX light element analysis of IDPs are described in detail elsewhere (Thomas et al., 1993b).

Following the initial bulk chemical analyses at JSC, multiple fragments were distributed to several research groups for the following analyses: mineralogical studies using transmission electron microscopy (TEM), noble gas measurements, trace element abundances by Synchrotron X-ray Fluorescence (SXRF), ion microprobe studies for isotopic compositions, microprobe two-step laser mass spectrometer (μL^2MS) for trace organic chemistry, and reflectance spectroscopy using a microscope photometer (Fig. 1).

TEM

Ten of the fragments and ten of the fines were embedded in epoxy, thin sectioned using an ultramicrotome, and examined with a JEOL

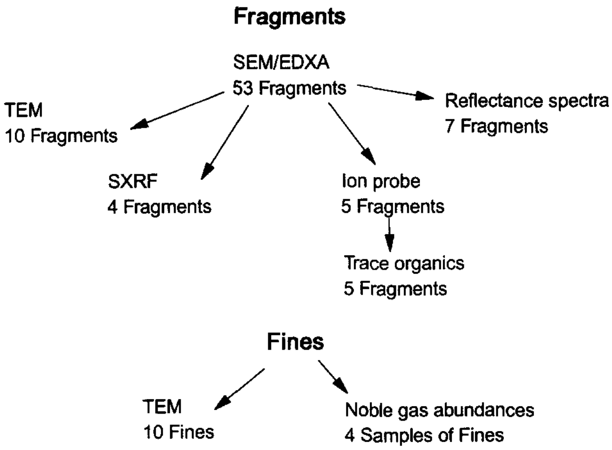

FIG. 1. Methods flowchart showing the types of analyses performed on fragments and fines from cluster L2008#5.

2000 FX TEM equipped with a Link EDX spectrometer. Modal mineralogy was determined for fragments and fines as described in Klöck et al. (1989).

Noble Gas Measurements

Helium content and the helium release temperatures for four samples were determined by step-heating experiments (technique described in detail by Nier and Schlutter, 1993). Each sample consisted of several fines, which approximate a fragment 10 μm in diameter. The fines, which were folded into a square of tantalum foil called an oven, were heated, the gas was extracted, and helium measurements were made by a mass spectrometer.

SXRF

This technique, which is particularly sensitive for the elements from chromium to bromine, was used to determine trace element abundances in four large fragments. The analytical method is described in detail by Flynn and Sutton (1991).

Ion Probe

The Washington University modified IMS-3f microprobe was used to determine hydrogen, carbon, and nitrogen isotopes of eight fragments. A primary ion beam of 8.5 KeV Cs^+ ions was used to analyze the fragments. Hydrogen, carbon, and nitrogen (measured as CN) were measured as negative secondary ions. Carbon and nitrogen isotopic measurements were performed at a mass resolving power of 5,500 and hydrogen isotopic measurements were performed at low mass resolution. Further details of the technique can be found in McKeegan et al. (1985).

Trace Organic Composition

Following ion probe analysis, the same fragments were analyzed for the presence of polycyclic aromatic hydrocarbons (PAHs). PAHs signatures were obtained with a μL^2MS (Kovalenko et al., 1992; Clemett et al., 1993).

Reflectance Spectra

Spectra over the visible wavelength range (380–800 nm) were acquired for seven fragments using techniques described by Bradley et al. (1994).

RESULTS AND DISCUSSION

Chemistry and Mineralogy

Table 1 shows normalized element abundances for fifty-three fragments analyzed from cluster L2008#5; ~25% of the fragments contain at least one major element with nonchondritic abundances. Table 2 shows the mean, standard deviation, and range of element abundances of all fragments. The cluster mean for all elements is chondritic, within a factor of two of CI, with the exception of minor elements sodium, phosphorus, and titanium which were ~4 × CI, ~5 × CI, and 2.5 × CI, respectively. The range of major elements (C, O, Mg, Si, S, and Fe) and the cluster mean are shown graphically in Fig. 2; large ranges for major elements suggest that compositional differences exist (also see Table 1). Chemical heterogeneity of individual

Table 2
Mean composition (wt.%) and range of element abundances of 53 fragments from cluster L2008#5. Bulk composition of Orgueil (CI) is shown for comparison.

	Cluster Fragments Mean and 1σ Variations (Wt.%)	Range	Bulk Composition of Orgueil (CI)* (Wt.%)
C	7 ± 3.7	1-29	3.5
O	34.0 ± 2.3	15.2-47.1	46.4
Na	1.9 ± 0.6	0.1-5.7	0.5
Mg	9.5 ± 0.9	0.5-20.6	9.5
Al	1.4 ± 0.2	0.1-10.6	0.9
Si	14.9 ± 0.7	0.9-30.0	10.7
P	0.6 ± 0.1	0.0-3.7	0.1
S	6.3 ± 4.2	0.2-25.6	5.3
K	0.1 ± 0.1	0.0-1.8	0.1
Ca	1.4 ± 0.1	0.0-13.8	0.9
Ti	0.1 ± 0.0	0.0-3.6	0.04
Cr	0.2 ± 0.1	0.0-0.9	0.3
Mn	0.2 ± 0.1	0.0-1.0	0.2
Fe	21.1 ± 0.5	0.9-57.6	18.5
Ni	1.2 ± 0.1	0.0-3.5	1.1

*Normalized without water; Anders and Grevesse (1989)

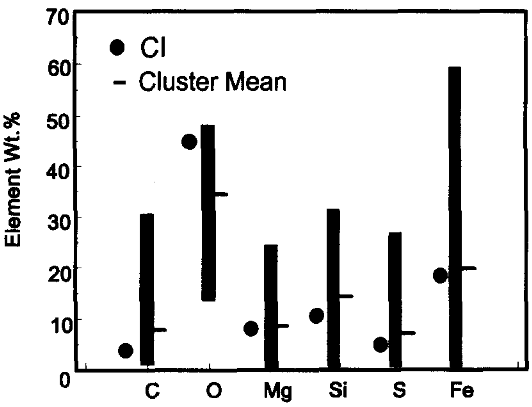

FIG. 2. Range and mean of major element abundances for fifty-three fragments from cluster L2008#5. Average values are also shown for Orgueil (CI). The range of element abundances varies widely among fragments; however, the cluster mean is chondritic (within 2 × CI).

cluster fragments is shown in a Si-Mg-Fe (atomic) triangular plot (Fig. 3). Individual fragments display a variety of compositions ranging from Si- to Fe-rich. More than 50% of the fragments plot in the region between the solid-solution tie lines for pyroxene and olivine; this region also represents solar abundances for these elements. Atomic Mg/(Mg + Fe) values range from 0.2–0.95 with the cluster average at 0.51 (Fig. 4).

Representative bulk EDX analyses of eighteen fragments are shown in Table 3. Fragments are grouped according to their chemical compositions; e.g., some fragments are clearly dominated by sulfides, magnetite, or carbonaceous material, while others have a bulk chondritic composition. In general, fragments dominated by sulfides have lower oxygen abundances, and sulfur and iron are > 2 × CI. In two fragments, Clu111 and Clu34, Ni is > 2 × CI suggesting that kamacite or Ni-rich iron sulfide (e.g., pentlandite) could be present. In the magnetite-dominated chemical group, sulfur abundance ranges from 1.0–7.8 wt% and Fe > 2 × CI. Of the representative fragments with chondritic element abundances, Clu51 has Ni > 2 × CI and S ~ 2 × CI; this fragment contains Ni-rich and Ni-poor iron sulfides. Mineralogy was determined for two of the chondritic fragments: Clu18 is composed primarily of fine-grained aggregates containing ~10 nm Fe metal and Fe-sulfide grains embedded in a silica-rich glassy matrix, while Clu51 contains a mixture of olivine and pyroxene grains (also see Table 3). Of the fifty-three fragments analyzed, twelve were carbon-rich fragments with C > 3 × CI (~11 wt%). All other major element abundances are within 2 × CI for the C-rich fragments.

For comparison to other published data, we have normalized some of our element abundances to silicon; the atomic abundance ratios to silicon for IDPs and other extraterrestrial materials are shown in Table 4. The average ratios of major elements are essentially the same for the cluster fragments, anhydrous IDPs, and 10–20 μm fragments of the Orgueil CI chondrite, with the exception of carbon. Although the heterogeneity is the same for cluster IDPs and other fine grained chondritic material (e.g., chondrite matrix), the grain size in IDPs is, in general, much finer than the grain size of chondrites. Some coarse (5–10 μm) fragments from both L2008#5 and Orgueil are nonchondritic (e.g., individual fragments are dominated by single minerals such as olivine, iron sulfides, etc.) unlike the fine-grained anhydrous IDPs, which have chondritic compositions.

Tables 5 and 6 list mineral assemblages found in ten large fragments and fines from cluster L2008#5. Fragments have been classified according to the most abundant mineral phase. A variety of mineral phases are present in this cluster particle, and minerals with similar compositional ranges are found in

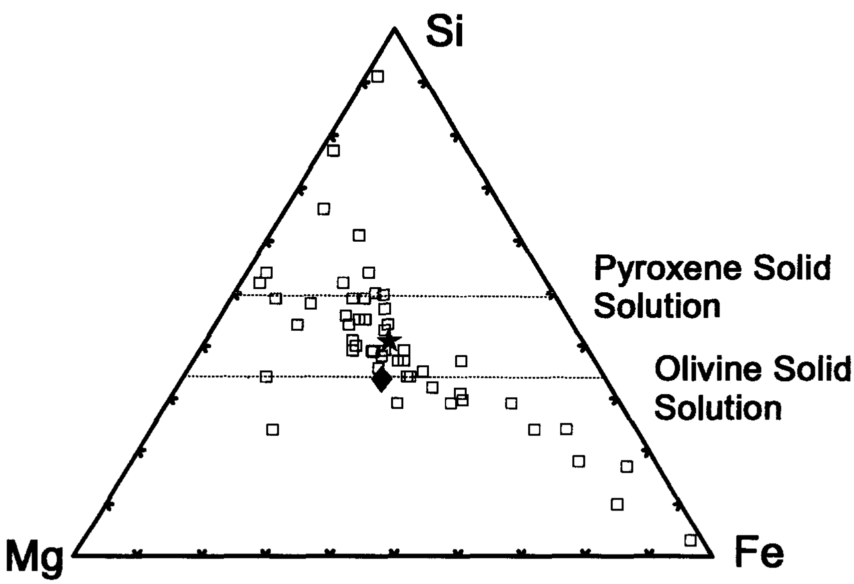

FIG. 3. Atomic abundances of Si-Mg-Fe for fifty-three cluster fragments are shown on a triangular plot. Fragments range in composition from Si- to Fe-rich. The cluster average is located between the olivine and pyroxene compositional tie lines indicating that L2008#5 is composed of a subequal mixture of olivine and pyroxene. The value for CI plots close to that for the cluster average. Key: □, cluster fragments; ★, cluster average; ♦, Orgueil (CI).

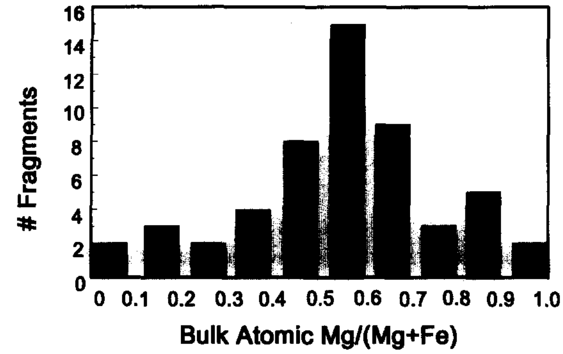

FIG. 4. Atomic Mg/(Mg + Fe) values for fifty-three fragments range from 0.2–1.0 with an average at 0.51. The mean value for Orgueil (CI) is 0.55.

large fragments and fines. For example, olivine compositions range from Fo 57–99 in large fragments and from Fo 66–98 in fines. However, several olivine-dominated fragments have ranges of olivine compositions which differ from one fragment to another (e.g., Clu35 and Clu317). Some fragments contain olivines with narrow ranges, or equilibrated compositions (e.g., Clu51 and Clu52, Fig. 5a) and others have olivines with large ranges, or unequilibrated compositions (e.g., Clu35 and Clu17, Fig. 5b).

Pyroxene compositions include enstatite and high-Ca pyroxenes. Low-Fe, Mn-enriched (LIME) silicate grains were observed in two fragments and one fine. Silicates with this unique composition have been previously reported from some anhydrous IDPs and chondritic meteorite matrices (Klöck et al., 1989). Fine-grained aggregates (FGAs), also known as unequilibrated aggregates (Bradley, 1994a), tar balls (Bradley and Brownlee, 1988), and GEMS (glass with embedded metal and sulfides; Bradley, 1994b) are the major constituents in two fragments (Clu52 and Clu17); they are observed as minor components in one fragment (Clu11) and two fines (#2 and #7). All FGAs in fragments and fines from L2008#5 are composed of a glassy matrix with embedded metal and sulfides. Fe-sulfides with Ni (FSN) are present in most fragments and fines.

Noncrystalline regions, typically <500 nm in size, composed of carbonaceous material or glass are present in some fragments. We observed amorphous, carbonaceous material in four fragments with C > 3 × CI. Carbonaceous material can have a smooth or vesicular texture (Fig. 6a,b); we did not observe carbonaceous material in the fines. Noncrystalline, noncarbonaceous solids have compositions which range from Si-rich to feldspathic with minor amounts of magnesium and iron present in some regions; some glassy regions contain considerable iron, up to 25 wt%. Glassy areas have either a smooth or a vesicular texture. Mineral grain sizes vary from fragment to fragment: of the twenty fragments and fines examined, nine have constituent grains that are predominantly coarse grained (~1 μm in diameter) (e.g., fragment Clu317, Fig. 7a), six are predominantly fine grained (<50 nm in diameter) (e.g., fragment Clu17, Fig. 7b), and five contain a mixture of coarse and fine grains. Partial magnetite rims were observed in fourteen of twenty fragments and fines from this cluster (e.g., fragment Clu17, Fig. 8).

Noble Gas Measurements

Helium content and helium release temperatures for four samples were determined by step-heating experiments. The four samples are fines estimated to make up a 10-μm sized fragment. The average ^{4}He abundance is ~4.1 (cc × 10^{11}) and the extraction temperatures for removal of 50% of the He range from 750–1040°C, with an average at 928°C (Table 7). In previous work on twenty individual IDPs, the average ^{4}He abundance was 4.6 (cc × 10^{11}) (Nier and Schlutter, 1992) which is close to the cluster average (Table 7). However, the range of ^{4}He is from ~0 (undetectable) to 17. The average ^{4}He abundance of 24 IDPs from unrelated, cluster IDPs is 4.7 (cc × 10^{11}) and the range is from 0.33 to 44.6 (Table 7, Nier and Schlutter, 1993). The 50% helium release temperature for these IDPs is 798°C. The average ^{4}He abundance is nearly identical for individual IDPs, unrelated cluster IDPs, and cluster L2008#5 fragments, indicating that the exposure history is similar for all three groups of IDPs. The range of ^{3}He/^{4}He exhibited by the individual and unrelated cluster IDPs is much larger than that of the L2008#5 cluster fragments, possibly due to the small number of fragments analyzed. The average 50% He release temperature for the cluster fragments is significantly higher than that of unrelated cluster IDPs (928 vs. 798°C, respectively) suggesting that this cluster was heated, on average, to higher temperatures during atmospheric entry. Helium release temperatures observed from our four cluster fragments are significantly different (750°C vs. a group ranging from 910–1040°C). The low helium release temperature of one fragment suggests that it was not strongly heated during atmospheric entry while the high release temperatures of three others suggest they were strongly heated; the range of fragment temperatures indicates that this cluster has likely maintained a thermal gradient during atmospheric entry, especially if the cluster was very porous and if it contained components subject to sublimation (e.g., organic material, water).

^{3}He/^{4}He ratios are given for three groups of IDPs, bulk carbonaceous and unequilibrated ordinary chondrites, and four samples of Nogoya (Table 7). The ^{3}He/^{4}He range for cluster L2008#5 is 3.3–7.2 (×10^4), which is within that for both groups of IDPs, as well as bulk CM, and CV chondrites.

SXRF

Four fragments from L2008#5 were analyzed by SXRF to determine trace element abundances. With the exception of zinc in one IDP, the individual fragments show variations of individual element abundances essentially spanning the entire range of individual analyses reported by Flynn et al. (1993) for all anhydrous IDPs. All fragments show deviations by more than a factor of two from CI for at least three elements (Fig. 9 and Table 8). The only consistent trends are enrichments in copper, selenium, and bromine, and a depletion in zinc relative to CI.

Two fragments show marked depletions in zinc (Zn/Fe < 0.1); Zn/Fe ratios range from 0.2–0.5 for the remaining fragments (Table 8). With the exception of the zinc depletion, which is seen in all fragments, there is no obvious pattern

Table 3
Representative analyses of sulfide-dominated, magnetite-dominated, chondritic, and carbon-rich fragments from cluster L2008#5. (Minor elements are excluded resulting in low totals).

Representative bulk analyses of sulfide-dominated fragments

Element Wt%	Clu38	Clu111	Clu22	Clu34
C	3	6	2	3
O	16.2	17.6	15.2	25.0
Mg	2.7	2.7	0.5	3.6
Si	3.0	6.8	0.9	5.8
S	25.6	25.3	23.4	12.4
Fe	47.8	36.9	57.6	46.0
Ni	0.5	3.5	0.2	3.0
Total	98.8	98.8	98.0	98.8

Representative bulk analyses of magnetite-dominated fragments

Element Wt%	Clu21	Glu117	Clu112	Clu37
C	4	1	2	3
O	29.1	31.5	28.2	30.2
Mg	4.4	5.1	1.3	8.8
Si	7.9	10.3	5.6	13.1
S	7.1	7.8	3.9	1.0
Fe	38.1	37.6	51.8	38.4
Ni	4.0	2.5	3.4	1.8
Total	94.6	95.8	96.2	96.3

Representative bulk analyses of chondritic fragments

Element Wt.%	Clu25	Clu24	Clu18	Clu28	Clu51	Clu116
C	7	5	4	9	4	2
O	35.6	40.3	34.8	36.3	32.3	33.2
Mg	11.7	11.8	12.2	10.5	9.2	9.7
Si	15.3	14.5	14.4	14.0	13.3	12.4
S	5.4	2.8	4.3	4.1	10.6	5.2
Fe	18.4	17.6	24.2	19.0	23.1	30.8
Ni	1.1	0.8	0.6	1.3	2.3	1.0
Total	94.5	92.8	94.5	94.2	94.8	94.3

Representative bulk analyses of carbon-rich fragments

Element Wt.%	Clu310	Clu313	Clu32	Clu33
C	29	15	17	23
O	29.8	37.1	34.0	30.3
Mg	8.1	9.3	8.7	7.1
Si	12.3	16.3	16.4	16.4
S	5.9	4.6	4.5	6.6
Fe	10.5	12.5	11.6	11.6
Ni	0.6	0.7	0.6	0.6
Total	96.2	95.5	92.8	95.6

suggesting genetic links between the fragments. Flynn and Sutton (1991) have previously reported the analyses of two stratospheric particles which were recovered from the collectors intact but which broke into several fragments before trace element analysis. One of these (L2003E1) separated into three fragments. All elements from chromium to selenium were within a factor of three of CI except Cr ($4.5 \times$ CI) in one fragment and selenium ($0.17 \times$ CI) in another fragment. Each fragment exhibited a similar bromine enrichment. These fragments of L2003E1 showed a much narrower range of variation in element abundances than did the fragments of cluster L2008#5. The second fragmented IDP (U2015G1) (Sutton and Flynn, 1988) exhibited significant compositional heterogeneity with Ni/Fe differing by a factor of three and the Zn/Fe differing by a factor of nine between the two fragments.

The zinc content of individual IDPs correlates well with other indicators of severe heating (Flynn et al., 1992; Keller et al., 1992; Thomas et al., 1992). Zinc is depleted relative to CI in all four fragments with two showing the very low Zn/Fe ratios suggestive of significant heating. The range of Zn/Fe ratios of Clu16 and Clu18 is an order of magnitude lower than that for fragments Clu21 and Clu319 indicating different degrees of heating between the pairs of fragments, assuming comparable initial zinc levels.

Despite the heterogeneity between fragments of this cluster, the average composition of the four fragments agrees well with the average previously reported by Flynn et al. (1993) for eight heated, anhydrous IDPs (Table 8, Fig. 10). The average composition of the cluster fragments shows the general enrichment of volatile elements relative to CI meteorites which is characteristic of smaller, individual IDPs (Flynn et al., 1992), with depletions in zinc and germanium consistent with significant heating (Flynn et al., 1994).

Isotopic Measurements

Ion microprobe measurements of hydrogen isotopes were performed on five fragments with a range of bulk carbon

Table 4
Comparison of atomic abundance ratios to silicon (ranges in parentheses) for cluster fragments, anhydrous IDPs, and other extraterrestrial materials

	L2008#5 Fragments[a]	Anhydrous IDPs[b]	Anhydrous IDPs[c]	Orgueil Fragments[b]	Orgueil[d]	CM Matrix[e]	CV Matrix[e]	UOC[f]	Comet Halley[g]
C	1.1	2.0	2.4	0.6	0.8				4.4
	(0.2-4.6)	(0.7-4.9)		(0.0-1.3)					
O	4.0	4.0	4.0	5.1	7.6				4.8
Na	0.2	0.1	0.05	0.09	0.05	0.04	0.02	0.12	0.05
Mg	0.7	0.8	1.0	1.0	1.0	1.0	1.0	0.5	0.5
	(0.04-1.6)	(0.5-1.8)	(0.6-2.0)	(0.04-1.2)					
Al	0.1	0.1	0.07	0.1	0.08	0.1	0.1	0.12	0.04
S	0.4	0.4	0.4	0.2	0.4	0.2	0.05	0.05	0.4
	(0.01-1.5)	(0.2-1.3)	(0.1-1.8)	(0.01-0.5)					
Ca	0.07	0.04	0.05	0.1	0.06	0.03	0.07	0.02	0.04
Cr	0.008	0.008		0.008	0.02	0.01	0.01		
Mn	0.008	0.008		0.004	0.01	0.006	0.006		
Fe	0.7	0.6	0.7	0.73	0.87	0.89	0.93	0.6	0.3
	(0.03-1.9)	(0.2-2.0)	(0.2-2.0)	(0.02-2.1)					
Ni	0.04	0.02	0.02	0.06	0.05	0.06	0.04	0.03	0.02

[a] This work.
[b] Thomas *et al.* (1993b).
[c] Schramm *et al.* (1989).
[d] Anders and Grevesse (1989).
[e] McSween and Richardson (1977). (CM, CV).
[f] Huss *et al.* (1981). (Semarkona).
[g] Jessberger *et al.* (1988).

abundances (Table 9). Three of the fragments were subsequently measured for carbon and nitrogen isotopes as well. Four C-poor fragments were obtained by crushing Clu37, which was previously determined to contain 3 wt% C. Subsequent EDX analysis confirmed that all subfragments had low carbon abundances. Four C-rich (10–29 wt%) fragments were analyzed as well. These included Clu110, Clu313, and two subfragments of Clu19, and nine subfragments of Clu310.

Deuterium enrichments (δD) were observed in three of the four C-rich fragments and range from +322 to +822 ‰ (Table 9). Three of the four C-rich fragments were also found to have ^{15}N enrichments of up to 260 ‰. No substantial carbon isotopic anomalies were observed.

Trace Organic Chemistry

Four fragments were analyzed for trace organic components using microprobe two-step mass spectrometry (μL^2MS) (Kovalenko et al., 1992). These fragments had been analyzed previously for D/H isotopic ratios using the ion microprobe technique described in the previous section. In the first step of μL^2MS, constituent molecules of the sample are desorbed with a pulsed infrared laser beam which is focused to microscopic dimensions. For this study, either a CO_2 laser (λ = 10.6 μm) or Nd:YAG laser (λ = 1.064 μm) was used, giving a spatial resolution of ~40 μm or ~5 μm, respectively. The choice of desorption laser is determined by the particle size and proximity of other fragments on the sample mount. Both lasers give similar mass spectra; the difference is the spatial profile. The laser power is kept low enough (~10^6 W/cm^2) to ensure desorption of neutral organic species with little or no fragmentation. In the second step, polycyclic aromatic hydrocarbons (PAHs) in the desorbed plume are preferentially ionized by a pulsed ultraviolet laser beam (Nd:YAG, λ = 266 nm) which passes through the plume. The wavelength provides selectivity through resonance enhanced multiphoton ionization according to mass.

PAHs were observed in several of the cluster fragments, most notably Clu19(β) and Clu110 (Table 9). Significant variability of the PAH signature was observed both among different fragment particles and among subfragments of the same particles. The variation in signal is partially correlated, as would be expected, to the size of the fragment, however there are clear exceptions. For example, a strong distribution of aromatic species was observed in Clu19(β) (Fig. 11), whereas no signal was observed in Clu19(α) above the detection limits of the instrument,† each fragment having approximately the same dimensions. The mass spectra of PAHs from those fragments show evidence of aromatic species which are very different from those of two previously studied unrelated IDPs, Aurelian (U47-M1-2a) and Florianus (U47-M1-7a) (Clemett et al., 1993). Both the mass range of aromatic species observed and the structural complexity are reduced, ranging primarily from one to six fused ring species with little indication of alkylation (replacement of -H with -$(CH_2)nCH_3$, where n = 0, 1, 2···). However, individual peak intensities in some cases (e.g., naphthalene and chyr-

† The detection sensitivity for a given PAH species depends both on its concentration in the sample and its photoionization cross section (Zenobi and Zare, 1991). The ultimate detection sensitivity for the molecule coronene (C_{24}, H_{12}, 300 amu) has been measured in the μL^2MS instrument to be 0.8 attomoles (~500,000 molecules in a 40 μm analysis spot), and that for the molecule phrenanthrene (C_{14}, H_{10}, 178 amu) ~0.02 attomoles (~12,000 molecules in a 40 μm analysis spot).

Table 5
Mineralogy of ten large fragments from cluster L2008#5

Fragment	Olivine	Enstatite	Pyroxene (Hi Ca)	FGA*	FSN**	C-type Material	Glass	Others	Mineral Grain Sizes (CG†, FG‡)	Mt Rim•
Olivine-Dominated										
Clu317	Fo 63-68; 1Fo 95				Rare	Not Obsv. 2 wt.%	Yes		CG	Yes
Clu11	Fo 79-84	Yes	Yes	Rare	Yes	Obsv. 14 wt.%			CG & FG	Yes
Clu35	Fo 57-82	Yes			Rare	Not Obsv. 2 wt.%	Yes	Chromite	CG & FG	Yes
Pyroxene-Dominated										
Clu13	1 Fo 88	~99%			Yes	Not Obsv. 3 wt.%		Kamacite	CG & FG	Yes
Clu315		Yes			Yes	Obsv. 15 wt.%		Fe Metal, Kamacite	FG	No
Olivine-Pyroxene Mix										
Clu51	Fo 84	Yes				Not Obsv. 4 wt.%	Yes		FG	Yes
FGA Dominated										
Clu52	Fo 95; LIME••	Yes; LIME••		Yes	Yes	Obsv. 13 wt.%			FG	No
Clu17	Fo 79-99	Yes		Yes	Yes	Obsv. 12 wt.%	Yes		FG	Yes
Others										
Clu38	Rare, Fo 65-76				Large, single	Not Obsv. 3 wt.%			CG	Yes
Clu318		LIME••			Rare	Not Obsv. 4 wt.%	Yes	Large Magnetite	CG	Yes

*Fine grain aggregate **Fe-Sulfide with Ni †Coarse-grained ‡Fine-grained •Magnetite Rim
••LIME Low iron, manganese-enriched (From Klöck *et al.*,1990).

sene/triphenylene) are more intense than the most intense peaks observed previously from Aurelian.‡ Additionally, spectra are dominated by even mass PAHs with little evidence of odd mass peaks observed in Aurelian and Florianus. The odd mass peaks were previously interpreted as nitrogen containing functional groups such as -CN or -NH_2 attached to an aromatic chromophore. It is likely that the distribution of PAHs observed in Clu19 and Clu110 may have been perturbed by prior exposure to the ion probe (10 KeV Cs^+ ions) used for the D/H measurements; however, as observed previously by Clemett et al. (1993), strong PAHs signals are only observed in deuterium-rich particles (also see Table 9). Deuterium enrichment alone does not necessarily indicate that PAHs will be present, but PAHs signals have only been observed on deuterium-rich particles. PAHs and elemental carbon coexist in some fragments of this cluster; however, considering the mass of the entire cluster, they appear to be inhomogeneously distributed.

‡ Care must be taken in comparing different mass peak intensities since ion intensities are not only proportional to the concentration of the compound in the sample, but also the photoionization adsorption cross section for that compound at the laser ionization wavelength (λ = 266 nm).

Reflectance Spectra

Visible wavelength reflectance spectra were acquired from seven individual fragments from cluster L2008#5 (Fig. 12). Fragments were randomly selected for maximum variability; some are chondritic while others are dominated by single mineral grains. All spectra show a rise into the red, similar to that in certain primitive asteroids, although two fragments (Clu33 and Clu313) exhibit a slight decline at ~800 nm. These two fragments are the most C-rich of the seven IDPs (Table 10). Reflectivity values range from 3–18% (Table 10 and Fig. 12). Two fragments with the highest albedos, Clu39 and Clu111, are dominated by large single mineral grains (Ca-rich pyroxene and Fe-Ni sulfide, respectively). Five fragments have albedos which are essentially indistinguishable:

Table 6
Mineralogy of ten fines from cluster L2008#5

Sample	Olivine	Enstatite	Pyroxene (Hi Ca)	FGA*	FSN**	C-type Material	Glass	Others	Mineral Grain Sizes (CG†, FG‡)	Mt Rim•
Olivine-Dominated										
1	Fo 78						Yes	Chromite	CG	Yes
2	Fo 85	Yes; 1 LIME••		Yes			Yes	Kamacite	CG & FG	Yes
3	Fo 86	Yes	Yes		Yes		Yes	Magnetite	CG	Yes
Pyroxene-Dominated										
4		Yes	Yes						CG	Yes
5			Yes		Yes				FG	Yes
Olivine-Pyroxene Mix										
6	Fo 66	Yes			Yes		Yes		CG & FG	Yes
FGA Dominated										
7	Fo 98		Yes	Yes	Yes				FG	No
Others										
8	Fo 68-91				Yes			Lg. Magnetite	CG	No
9					Yes			Lg Magnetite & Kamacite	CG	No
10		Yes			Yes		Yes	Kamacite Chromite Ferrihydrite	CG	No

*Fine grain aggregate **Fe-Sulfide with Ni †Coarse-grained ‡Fine-grained •Magnetite rim
••LIME Low iron, manganese-enriched (From Klöck *et al.*,1990).

Clu313, Clu33, Clu23, Clu37, and Clu111 (Fig. 12). The bulk carbon abundance ranges from 3–23 wt% for these five fragments. Although the two C-rich fragments (Clu33 and Clu313) have low albedos, other fragments which have chondritic carbon abundances exhibit nearly identical albedos (Clu37 and Clu23). Clu37 is probably dominated by magnetite; this fragment has 38.4 wt% Fe and ~1 wt% S (Table 3). Clu23 is chondritic for all major elements although sulfur is approaching 2 × CI abundance, suggesting iron sulfides are present. Fragment Clu312 has the lowest albedo and has chondritic abundances for all elements. Our data suggest that several criteria (carbon content, chemical, and mineral abundances) influence albedos and slopes of reflectance spectra.

The average reflectance spectrum for the seven fragments of L2008#5 is shown in Fig. 13a. The reflectance (~8% at 550 nm) and spectrum shape are comparable to spectra from several carbonaceous chondrites (5–10%; e.g., Hiroi et al., 1993). Reflectance spectra for "typical" S, M, C, P, and D asteroids are shown in Fig. 13b (Zellner et al., 1985). The average spectrum for the seven fragments shows differences from the spectra of common asteroids. The average cluster spectrum has a lower albedo and lacks the reddened slope of S-type asteroids, and is significantly brighter than the P- and D-type spectra; however, analyzed fragments were selected based on their diverse bulk chemical abundances which emphasizes interfragment variations of albedos.

DISCUSSION AND IMPLICATIONS

In the following sections we discuss and summarize some of the more important observations associated with cluster particle L2008#5: (1) the types of carbonaceous materials, including bulk carbon, carbon and nitrogen isotopes, PAHs, and the coexistence of these carbonaceous phases within a fragment, (2) the interfragment variability of carbonaceous materials, (3) cluster heating during atmospheric entry, (4) possible sources for this cluster based on our estimations of size, porosity, entry velocities, and reflectance spectra, and (5) our hypothesis that this cluster is a breccia based on the physical and chemical variations between fragments.

Carbonaceous Phases

Bulk carbon abundances

Carbon abundance ranges from 2–29 wt% (see Tables 1, 2, and Fig. 2). The cluster average is 7 wt% C which falls within the range exhibited by CI chondrites. Carbonaceous material is observed in TEM thin sections of fragments with

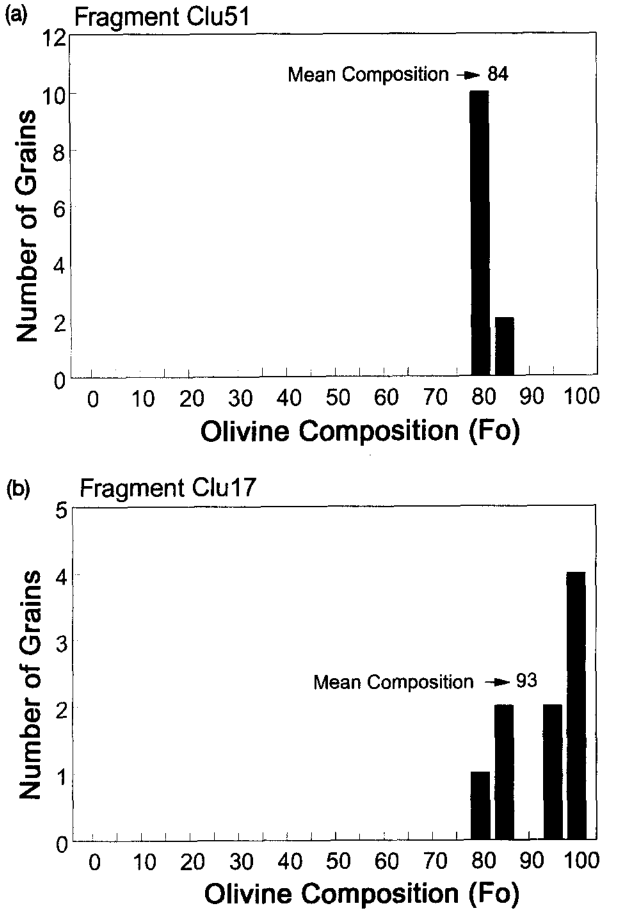

FIG. 5. Olivine compositions in two fragments from cluster L2008#5. (a) Fragment Clu51 contains olivines with equilibrated compositions which range from ~Fo 80–85 with an average at ~Fo 84. (b) Fragment Clu17 contains olivines with unequilibrated compositions; olivines range from ~Fo 80–100 with an average at Fo 93.

C > 3 × CI. The C-rich material is amorphous or poorly crystalline and in some instances exhibits vesicular textures. The amorphous carbon material is not distributed equally among fragments (see Table 5, carbonaceous material). For example, coarse-grained fragments tend to be C-poor (<5 wt% C), while those rich in FGAs have high carbon contents (~12 wt% C). However, amorphous carbonaceous material is still rather evenly distributed in C-rich fragments; it acts as a matrix holding individual grains together (Figs. 6a,b, and 14).

Isotopic and PAH measurements

We investigated the chemical state of the carbon in fragments with bulk carbon abundances ranging from 3–29 wt% by two complementary techniques: ion microprobe measurements of hydrogen, carbon, and nitrogen isotopes of each fragment and μL^2MS measurements which are exceptionally sensitive to the presence of PAHs.

We found substantial D enrichments in most of the C-rich fragments analyzed with enrichments ranging from +322 to +822‰. The apparent correlation of D enrichments with carbon content supports the assertion by McKeegan et al. (1985, 1987) that the D-rich carrier phase in IDPs is organic and not water of hydration. This degree of D enrichment appears to be too great to be caused by known solar system processes (Geiss and Reeves, 1981). The enrichment is commonly considered to be due to the partial retention of much larger enrichments of precursor molecules which formed in a presolar molecular cloud from ion-molecule chemistry.

Since the isotopic measurements were made on bulk samples, and μL^2MS measurements may reflect a relatively small fraction of the total organic matter present, it is not possible to identify the isotopic analyses with the PAHs observed in a given particle. However, to date, strong PAH signals have

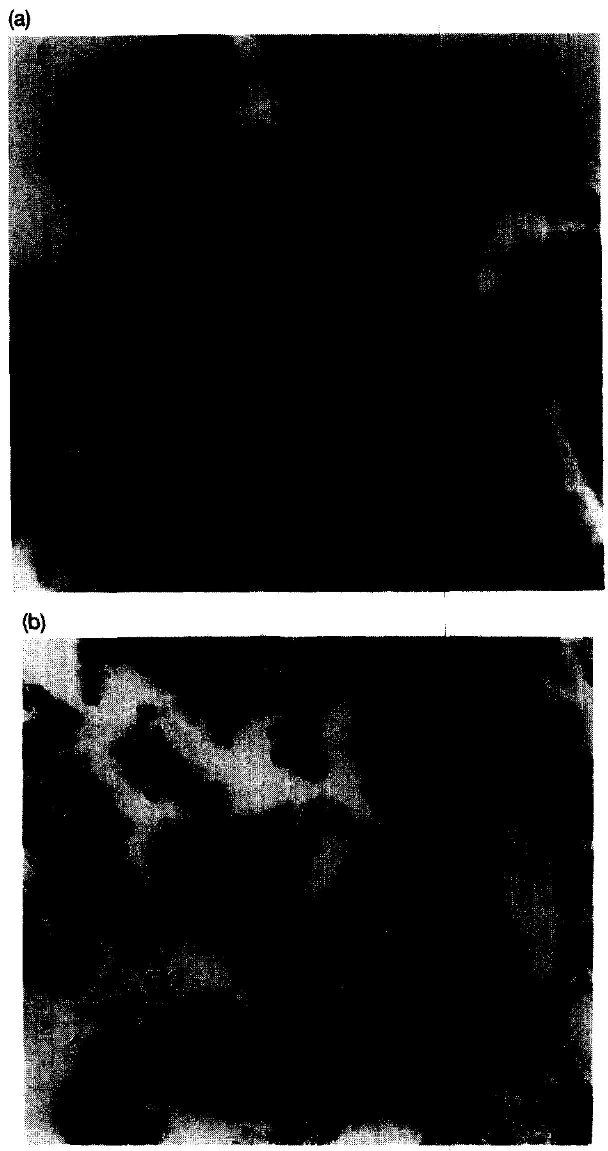

FIG. 6. TEM photomicrographs of thin sections of two fragments from cluster L2008#5. (a) Carbonaceous material (C) in fragment Clu17 has a vesicular texture. This fragment contains fine grain aggregates (FGAs); epoxy (E) is used as the embedding medium. (b) A lower magnification TEM image of carbonaceous material in fragment Clu52. The texture of the carbonaceous regions is vesicular which suggests that another phase, possibly polycyclic aromatic hydrocarbons (PAHs), was lost due to heating during atmospheric entry.

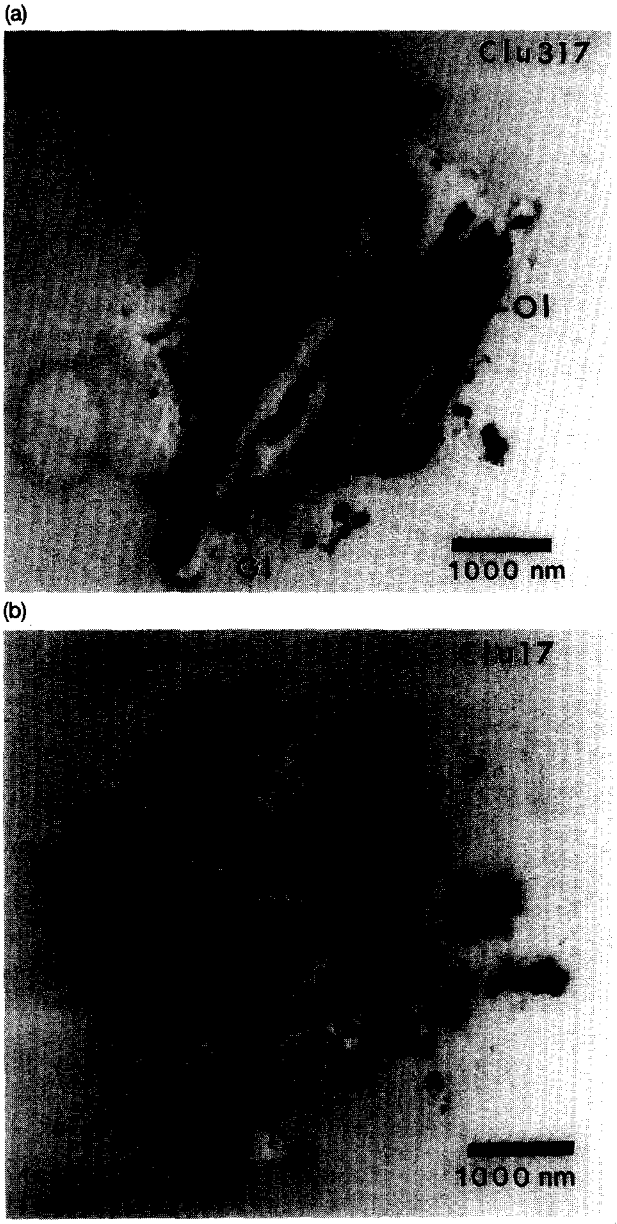

FIG. 7. Low magnification TEM photomicrographs of thin sections of two fragments from L2008#5. (a) Fragment Clu317 is coarse-grained and composed mainly of olivines and glass; light gray areas of epoxy surround the fragment thin section. (b) Fragment Clu17 has a fine-grained, primitive texture and contains mainly carbonaceous material, pyroxene, iron sulfides, and fine-grain aggregates (FGAs).

only been observed in deuterium-rich particles (Clemett et al., 1993; this work). Deuterium enrichments have been observed in every class of organic molecules that has been analyzed in Murchison including PAHs (Pizzarello et al., 1991; Krishnamurthy et al., 1992; Cronin et al., 1993).

We also found substantial ^{15}N enrichments in both fragments yielding strong PAH signals (Table 9). ^{15}N enrichments are expected to result from low temperature ion-molecule chemistry, but to a much smaller degree than the observed D enrichments (Adams and Smith, 1981). Substantial ^{15}N enrichments have been previously observed in IDPs (Stadermann et al., 1989), and a number of primitive meteorites (Kerridge 1985; Ash et al., 1993). Although the precise carrier phase(s) is not well constrained, ^{15}N enrichments appear to be associated with organic matter (Ash et al., 1993). It is interesting to note that two of the three IDPs observed to have strong PAH signals also carry ^{15}N enrichments (Clemett et al., 1993), though as in the case of the D enrichments, more work will be required to establish possible links of isotopic anomalies with PAHs in IDPs.

PAHs appear to be distributed heterogeneously throughout the cluster and do not seem to be correlated with any particular phase, although there is a rough correlation with size for those fragments showing evidence of PAHs. The mass distribution of PAHs is unique and has not been observed previously by μL^2MS on either chondritic meteorites or IDPs. We observed vesicular textures in the carbonaceous regions of some fragments of this cluster that were not analyzed individually by μL^2MS; this texture has been observed previously in other C-rich IDPs (Thomas et al., 1993b, 1994). A vesicular texture may be a consequence of evaporative loss of low-mass PAHs during a heating event; the heating event probably includes atmospheric entry and/or by ion bombardment during isotope analysis in the case of Clu19 and Clu110. Atmospheric entry heating is anticipated to effect PAHs in three ways: (1) they may be volatilized possibly recondensing on other fragments, (2) they may be fragmented with only some of the organic molecules being volatilized, or (3) they may undergo free-radical polymerization leading to involatile complex higher molecular weight species (Lewis, 1979; Greinke and Lewis, 1984). Since some of the cluster fragments contain PAHs with masses ranging from 400–500 amu, which are higher than the aromatic structures observed by μL^2MS in both ordinary and carbonaceous chondrites, these may be either compounds unique to IDPs or the product of the polymerization of lower molecular weight species. In the latter case, the PAH distributions may provide clues as to the degree of thermal processing experienced by an IDP during atmospheric entry.

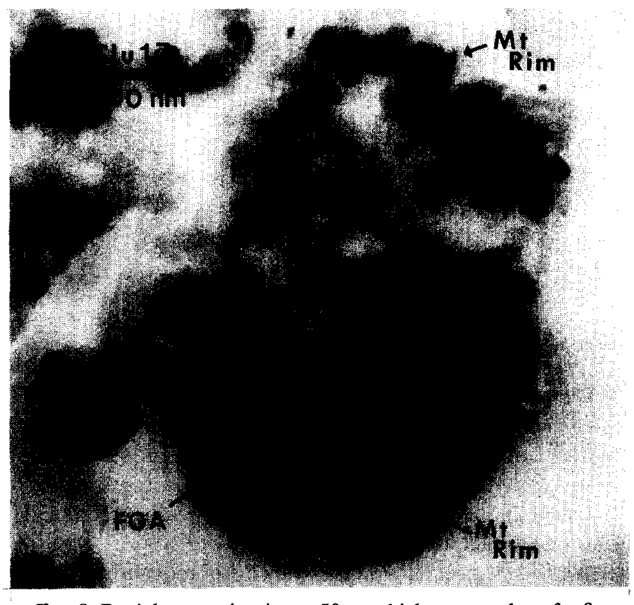

FIG. 8. Partial magnetite rim, <50 nm thick, on an edge of a fine-grained region of fragment Clu17.

Analysis of acid residues for PAHs in seventeen ordinary and carbonaceous chondrites (Clemett et al., 1992) shows that there are notable differences in both the distribution of parent PAHs and the degree of alkylation between the chondrite classes. This is interpreted to be a consequence of secondary processing such as thermal metamorphism and/or aqueous alteration on the original PAH distribution. Over fifty different molecular species have been detected in the chondritic residues, and none have masses significantly larger than 300 amu. This predominantly low-mass distribution is different from the cluster fragments which have PAHs with masses greater than 400 amu.

Heating Summary of Cluster Fragments

Four criteria were used to determine the extent to which L2008#5 was heated during atmospheric entry: (1) the presence of magnetite rims, (2) helium content and helium release temperatures, (3) SXRF trace element abundances, and (4) bulk sulfur content. Magnetite rims form on the exposed surfaces of grains located on the perimeter of the particle during entry into the Earth's atmosphere (Keller et al., 1992). We have observed partial, discontinuous magnetite rims on most cluster fragments and fines. However, we did not find magnetite rims on every fragment or fine. The TEM results suggest that (1) the cluster particle was uniformly heated and only developed magnetite on its exposed surfaces resulting in a diffusional gradient or (2) a thermal gradient was maintained by the cluster such that only the exterior surfaces were strongly affected during entry heating. The variability of helium release temperatures supports the latter interpretation in that most fragments contain little helium and have correspondingly high release temperatures, although one fragment has a release temperature that is significantly lower than the majority. The low abundances of some volatile trace elements (e.g., zinc) also suggest that some fragments have been strongly heated (as indicated by a major depletion in zinc) while other fragments retain chondritic levels of zinc. Seven fragments, with chondritic abundances for other major elements, show depletions in bulk sulfur (Table 1). If these frag-

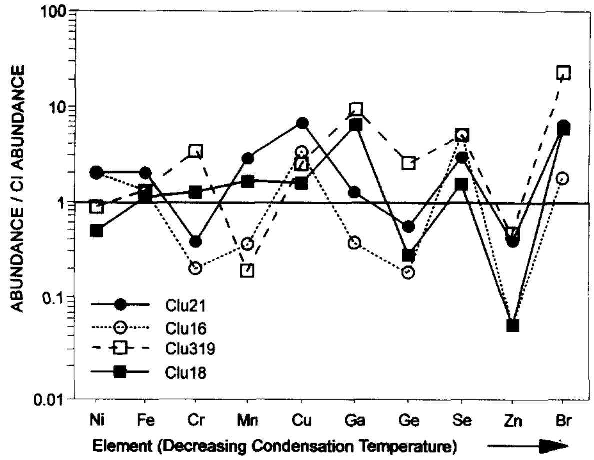

FIG. 9. Average CI normalized trace element abundances in four cluster fragments. Elements are ordered with decreasing nebula condensation temperature. Although element abundances show variation among fragments, some trends are apparent such as enrichments in copper, selenium, and bromine and depletions in zinc.

Table 7
He measurements of fines from cluster L2008#5 and other extraterrestrial materials

Sample	^{4}He (cc x10^{11})	50% He Release Temp. (°C)	^{3}He/^{4}He (x10^4)
IDPs			
1	4.5	750	3.3 +/- 0.7
2	6.1	1040	4.7 +/- 0.5
3	3.4	1010	7.2 +/- 1.2
4	2.2	910	5.9 +/- 1.4
Average	4.1	928	
Average of 20 individual IDPs*	4.6		
Range*	~0-17		1.9-6.4
Average of 24 unrelated cluster IDPs**	4.7	798	
Range**	0.33-44.6	550-1020	2.6-200
Meteorites			
Bulk Orgueil and Ivuna (CI)†			1.4-5.8
Bulk Murray, Mighei, Nogoya (CM)†			1.7-34.1
Bulk Ornans and Kainsaz (CO)†			109-154
Bulk Vigarano, Mokoia, Allende (CV)†			1.5-18.7
Nogoya (CM), 4 samples‡			1.7-3.4
Unequilibrated Ordinary Chondrites†			66-231

* Nier and Schlutter (1992)
** Nier and Schlutter (1993)
†Schultz and Kruse (1989)
‡Black (1972)

ments are assumed to have originally contained chondritic abundances of sulfur, then they have experienced sufficient heating during atmospheric entry to drive off some of the sulfur. Although theoretical models would predict that thermal gradients in particles < 100 μm in diameter are difficult to achieve and maintain, recent calculations suggest that endothermic reactions have a significant effect in moderating heat transfer from the particle surface to the core (Flynn, 1995). If so, then, we may be seeing evidence of a thermal gradient in an anhydrous IDP.

What is the Source of Cluster L2008#5?

Although the relative proportion of cometary and asteroidal dust entering the Earth's atmosphere has not been established, it is widely believed that near-Earth gravitational enhancement favors collection of IDPs that are of asteroidal origin (Flynn, 1990, 1994). Brownlee et al. (1993) suggest that up to 80% of IDPs which range in size from 5–15 μm in diameter originate from asteroidal bodies while the remaining ~20% are derived from objects in cometary orbits. In order to determine possible sources for this cluster, we need to calculate possible entry velocities; if the velocity value is less than or equal to 15 km/s, then it is more likely that the cluster is of asteroidal origin (Flynn, 1989). Although we do not know the original size of the parent particle for cluster L2008#5, we can put reasonable limits on its prefragmentation size in order to estimate the potential entry velocity. Here let us consider three models to constrain the pre-entry size, porosity, and density of L2008#5. We make the following assumptions for Model 1 (Fig. 15): (1) there is essentially no porosity between fragments and intrafragment porosity is low so the original size of the cluster is based on summing the volumes of individual fragments; this assumption leads to the estimate that the cluster would be ~40–50 μm in diameter assuming a spherical shape; (2) the initial density was ~2 g/cm^3 based on the mineralogy and observed porosity in microtome thin sections of the fragments; and (3) the cluster survived passage through the stratosphere without being heated to more than 1350°C, the approximate temperature at which chondritic material would melt and ablate (Love and Brownlee, 1994); we did not observe partial melting of any mineral grains in any fragments of L2008#5. Using the assumptions for Model 1, a cluster IDP 40–50 μm in diameter would yield peak Earth encounter velocities of 15–16 km/s according to thermal models for atmospheric entry heating (e.g., Love and Brownlee, 1994). This velocity range is consistent with an asteroidal or cometary origin for this cluster; it includes velocities for asteroidal particles and the lowest possible velocity for cometary particles. Model 1 places an upper limit on the entry velocity because no interfragment porosity was considered and the highest possible entry temperature was used. However, the cluster probably had a certain degree of porosity because it fractured (along weak junctions between fragments) into many fragments and fines on the collection surface.

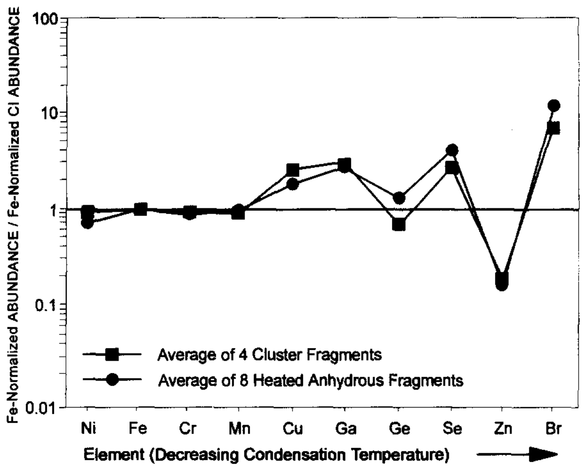

FIG. 10. Comparison of Fe-normalized element abundance/Fe-normalized CI abundance of the average of four cluster fragments and eight heated, anhydrous IDPs (from Flynn et al., 1993). The plots are nearly identical for all elements for both groups of IDPs.

In Model 2, we use more reasonable estimates of entry temperature, porosity, and density consistent with the mineralogical data. A better estimate of entry temperature would be from observations of magnetite formed on fragment surfaces and the 50% helium release temperature. Magnetite rims were found on many fragments and fines; they are generally thought to be formed over a range of temperatures, on the order of ~600–1000°C. The 50% helium release temperature may be a truer estimate of the peak temperature experienced during atmospheric entry of small particles (Brownlee et al., 1995). The highest 50% helium release temperature for this

Table 8
SXRF trace element abundances normalized to CI of 4 large fragments from cluster L2008#5 compared with abundances from 8 individual, heated IDPs.

Sample	Cr	Mn	Fe*	Ni	Cu	Zn	Ga	Ge	Se	Br	Zn/Fe
Clu16	0.2	0.4	1.4	2.0	3.5	0.06	0.4	0.2	6.1	2.0	0.04
Clu18	1.3	1.8	1.3	0.5	1.7	0.06	7.1	0.3	1.8	7.3	0.05
Clu21	0.4	3.1	2.1	2.0	7.4	0.44	1.4	0.6	3.4	7.3	0.2
Clu319	3.5	0.2	1.1	0.9	2.6	0.52	10.0	2.8	5.4	24.8	0.5
Fragment Average	1.4	1.4	1.5	1.4	3.8	0.3	4.7	1.0	4.2	10.4	0.2
Average of 8 Anhydrous IDPs**	0.8	1.0	1.0†	0.8	1.9	0.2	3.0	1.3	4.2	12.4	0.2

*Values from EDS
†Fe-normalized
**Flynn *et al.* (1993).

Table 9

Bulk carbon abundance (Wt.%), Deuterium (δD), ^{13}C enrichments, ^{15}N enrichments, and the presence of PAHs signatures in several large fragments from cluster L2008#5. Deuterium abundances are also given for bulk carbonaceous and unequilibrated chondrites.

Sample	C (Wt.%)	δD (per mil)*	$\delta^{13}C$ (per mil)	$\delta^{15}N$ (per mil)	μL^2MS **
IDPs					
Clu310(α)•	29	+89 ± 77			<5
Clu310(β)•	29	+56 ± 83			<5
Clu310(χ)•	29	+71 ± 75	-4 ± 7	+89 ± 27	<5
Clu310(δ)•	29	+66 ± 75	-8 ± 7	+56 ± 33	<5
Clu310(ε)•	29	+17 ± 79	-32 ± 9	+61 ± 32	<5
Clu310(ϕ)•	29	-14 ± 72			<5
Clu310(γ)•	29	-35 ± 6	-16 ± 13	+125 ± 36	<5
Clu310(η)•	29	-55 ± 18	-22 ± 27	+136 ± 38	<5
Clu310(ι)•	29	+44 ± 27			<5
Clu313†	15	+322 ± 67			Not Measured
Clu19(α)‡	14	+664 ± 84	-16 ± 26	+260 ± 34	<5
Clu19(β)‡	14	+424 ± 71	-33 ± 5	+202 ± 16	100
Clu110	10	+822 ± 91	-18 ± 10	+180 ± 18	43
Clu37(α)§	3	-24 ± 17			20
Clu37(β)§	3	+25 ± 22			7
Clu37(χ)§	3	-14 ± 36			32
Clu37(δ)§	3	+12 ± 29			13
Meteorites					
Bulk Carbonaceous Chondrites (CI)•		+44 to +300			
Bulk Carbonaceous Chondrites (CM)•		-176 to +990			
Bulk Carbonaceous Chondrites (CO)•		-116 to +2150			
Bulk Carbonaceous Chondrites (CV)•		-77 to +440			
Bulk Unequilibrated Ordinary Chondrites••		-77 to +3109			

* Terrestrial range is -200 to +50 per mil
** Integrated signal intensity from 80-450 amu normalized relative to Clu19 (β) = 100
• Clu310 broke into 9 separate pieces (α, β, χ, δ, ε, ϕ, γ, η, ι); analyzed by YAG desorption laser
†3 μm fragment too small for PAHs analysis
‡ Clu19 broke into 2 separate pieces (α & β)
§ Clu37 fractured into 4 pieces (α, β, χ, δ)
•Kerridge (1985)
••McNaughton *et al.* (1981)

cluster is 1040°C (Table 7), and considering the errors associated with the measurement, we are using 1100°C as the maximum entry temperature for Model 2. We previously assumed that our original cluster was 50 μm in diameter and had a density of 2 g/cm^3 with essentially no porosity (Fig. 15). Although fragments from this cluster display a range of porosities (i.e., coarse- and fine-grained fragments have widely divergent porosities), they average ~50%. This porosity is consistent with values estimated for other chondritic porous IDPs (e.g., Flynn and Sutton, 1990), although there are reports of IDPs with much lower densities (~0.1 g/cm^3, Rietmeijer, 1993; ~0.3 g/cm^3, Love et al., 1994). For Model 2, our estimate of density is ~1 g/cm^3 based on the same mass as used in Model 1 but incorporating the 50% porosity estimate. With these assumptions, the estimated prefragmentation diameter would be 63 μm (Fig. 15). Further increases in the estimated porosity result in lower densities. For example, a cluster with a porosity of 75% has a density of 0.5 g/cm^3 and a diameter of ~80 μm. In Model 2, assuming the peak temperature is 1100°C, then the entry velocity of the cluster is < 14 km/s, which is consistent with an asteroidal origin (see Love and Brownlee 1994; a 30 μm particle with a density of 2 g/cm^3 is treated the same as a particle 60 μm in diameter with a density of 1 g/cm^3). A cluster with a density 0.5 g/cm^3 and ~80 μm in diameter would have an entry velocity < 13 km/s. In fact, as the density decreases and the size of the cluster increases, the probability rises that this cluster is from an asteroidal source. Previous results from Love and Brownlee (1991) imply that virtually all of the unmelted micrometeorites > 70 μm in diameter are asteroidal in origin, considering there is no contribution from low velocity comets. We agree with others (e.g., Brownlee et al., 1995) that the 50% helium release temperature may vary with the presence of differing mineral phases and particle porosity so it cannot be precisely related to the peak temperature reached during atmospheric entry; however, our best estimate of size, density, entry temperature, and velocity for this cluster suggest that L2008#5 is very likely an asteroidal IDP.

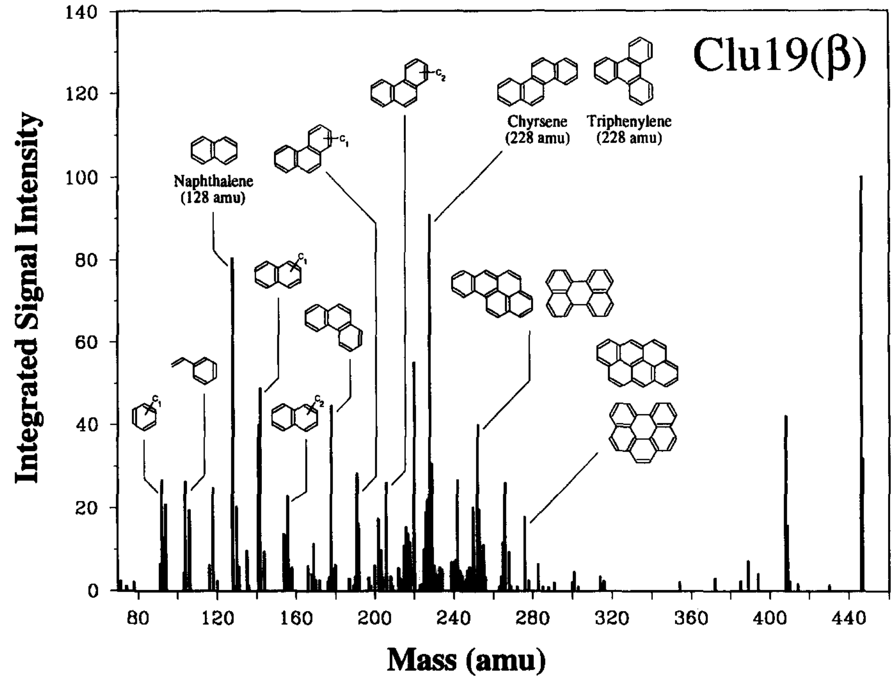

FIG. 11. The μL^2MS spectrum of the cluster particle Clu19(β), for the purposes of display, the signal intensities have been integrated over the mass range of $-1/2$ to $+1/2$ amu for each mass unit and the resulting data plotted as a histogram. The spectrum was generated from thirty single shot time-of-flight spectra (mass resolution ~ 1500), where each single-shot spectrum was stored in a computer, and later calibrated and co-added. Spectra assignments of a few of the more prominent parent PAH species and their alkylated homologs have been indicated. No peaks higher than 450 amu were observed.

Is Cluster L2008#5 a Breccia?

Our data on cluster L2008#5 show that it is clearly heterogeneous on a scale of 10–15 μm, the scale represented by the individual analyzed fragments. This heterogeneity includes both mineralogy and chemistry. While about 25% of the fragments are clearly dominated by a single large mineral grain such as iron sulfides or magnetite, most fragments consist of fine-grained material. Much of the heterogeneity results from differences from region to region within the cluster of the relative abundances of fine-grained mineral, glass, and carbonaceous material. For example, some fragments are rich in fine-grained olivine or pyroxene, others are rich in carbonaceous material, and others are rich in FGAs. If we did not know that these fragments came from the same cluster, we would probably consider that the fragments came from totally different parent sources.

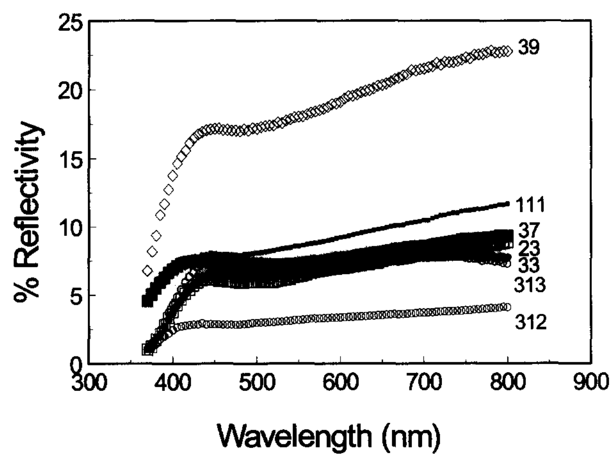

FIG. 12. Reflectance spectra over the visible wavelength range (380–800 nm) of seven fragments from cluster L2008#5. All spectra show a rise into the red; the albedos range from 3–23%. Fragment Clu39, which has the highest albedo, is composed mainly of a single clinopyroxene grain. Fragment Clu312, with the darkest albedo, has a chondritic composition for all major elements including carbon. Fragments Clu111, Clu37, Clu23, Clu33, and Clu313 do not have significantly different albedos although the carbon content is highly variable. For example, bulk carbon is ~3 wt% in Clu37, ~15 wt% in Clu313, and ~23 wt% in Clu33.

Earlier we showed that chondritic fragments have markedly different mineralogies. Chondritic fragments are dominated by olivines, by pyroxenes, by FGAs, or by a mixture of olivine and pyroxene grains (Tables 5 and 6). Furthermore, within a fragment, the olivines may be mostly unequilibrated showing

Table 10
Reflectivity (%) and bulk carbon abundance of seven fragments from cluster L2008#5

Fragment	% Reflectivity (at 575 nm)	C (Wt.%)
Clu312	3	9
Clu313	6	15
Clu33	6	23
Clu23	6.5	7
Clu37	7	3
Clu111	8	6
Clu39	18	3

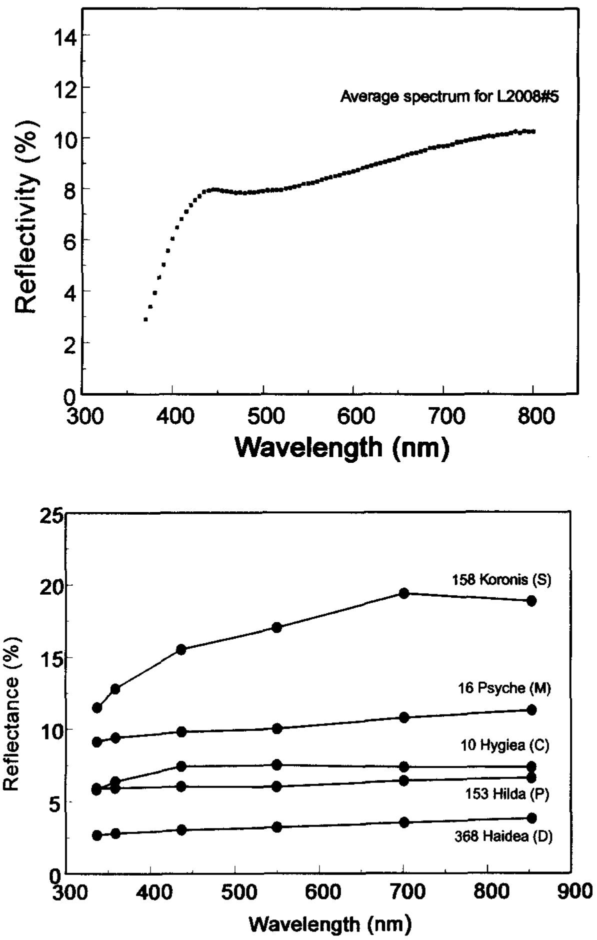

FIG. 13. Comparison of reflectance spectra for cluster L2008#5 and "typical" asteroids. (a) The average reflectance spectrum for seven fragments from cluster L2008#5. (b) Spectra for typical C-, D-, M-, P-, and S- type asteroids. S-type asteroids have reddened slopes and P- and D-type spectra are significantly darker than the average cluster spectrum (ECAS data from Zellner et al., 1985; Albedos from Tedesco, 1989).

a wide range of compositions or, by contrast, may have a narrow range of equilibrated compositions. Olivines from fine-grained fragments with "primitive textures," such as Clu17, have unequilibrated compositions which range from ~Fo 80–100 (Fig. 5b). In general, these fine-grained fragments are predominantly composed of pyroxene, FGAs, and carbonaceous material (Figs. 6a,b, and 7b). Clu51 is an example of a fragment with a coarse-grained texture; it contains equilibrated olivines with mean compositions of ~Fo 84 (Fig. 5a). *The presence of some fragments with fine-grained textures and unequilibrated mineralogies and other fragments with coarse-grained textures and equilibrated mineralogies suggests that cluster L2008#5 is really a breccia containing a physical mixture of material which has had significantly different histories.*

We consider three plausible mechanisms which can produce the heterogeneity we observe in fragments of L2008#5: (1) mixing of IDPs on the collection surface, (2) mixing of diverse mineral grains in the solar nebula, or (3) combining different lithologies from an asteroidal parent body (McKay et al., 1989). First, there is a possibility that the chemical and

FIG. 14. Fine-grain aggregates (FGAs) embedded in carbonaceous material (C). This texture is typical of carbon-rich fragments in cluster L2008#5 and other fine-grained anhydrous IDPs with C abundance > 3 × CI (Thomas et al., 1994).

mineralogical heterogeneities observed in L2008#5 could be the result of multiple impacts of different IDPs on the same location of the collection surface. However, we believe that all of the fragments are related to the same cluster because (1) the mineralogical and textural heterogeneity of the large fragments is duplicated in the fines, (2) the observed degree of heterogeneity is comparable to that observed in other cluster particles (Thomas et al., 1993a), and (3) the L2008 col-

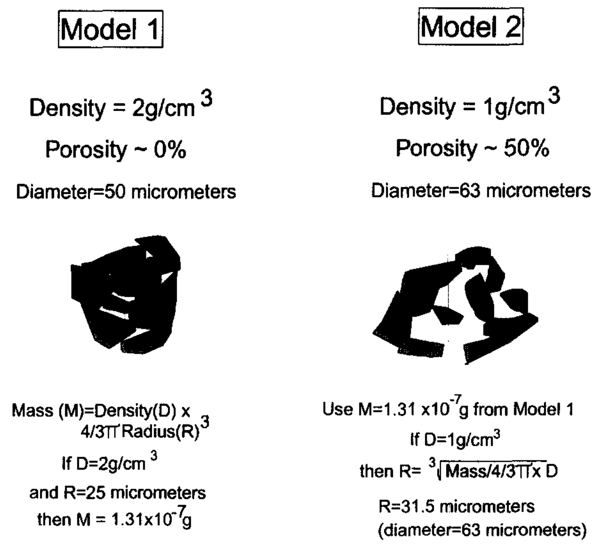

FIG. 15. Cartoon showing the effect of density upon size of a cluster particle. The particle has an assumed spherical shape (Volume = $4/3\pi R^3$). In Model 1, the mass is calculated for a particle having a diameter of 50 μm, density = 2 g/cm^3, and essentially no porosity (Mass = Volume × Density); this is our first estimation of cluster size. In Model 2, the mass calculated in Model 1 is used to determine the size of a particle with a density of 1 g/cm^3 and a porosity of 50%; a diameter of 63 μm is calculated for a cluster particle with the stated characteristics.

lection surface contained a low loading of IDPs and little background material, such as ash or aerosol particles. The fragments associated with L2008#5 were estimated to cover a surface area of $\sim$100 μm^2 on the collector. According to recent work by Flynn (1994), assuming a specific particle density on the collector, the surface area covered by this cluster could have been impacted with, at most, one contaminant fragment $\sim$5 μm or less in diameter.[§] If true, this contaminant fragment would constitute a very small proportion of the cluster. We conclude that essentially all of the analyzed fragments were originally part of the same large cluster.

We have shown that cluster L2008#5 exhibits fine scale heterogeneities in most of its chemical and mineralogical properties; we are left to speculate whether the heterogeneity in this cluster is a reflection of nebular or parent body processing. The fine-scale heterogeneity may have been generated during dust accretion in the early solar nebula. Thus, diverse mineral grains and carbonaceous materials were mixed, accreted, and little changed from that point forward. Alternatively, the heterogeneity may have resulted by mixing of different lithologies on an asteroidal parent body. These differences provide information on the potential parent body for the cluster and may indicate from which region within the parent body the cluster was derived. The cluster particle is anhydrous, and so it apparently escaped the effects of aqueous alteration. In addition, the cluster, in its entirety, has not equilibrated (e.g., magnesium abundances of olivines and pyroxenes are still highly variable; see Fig. 4), thus precluding any significant post-accretional thermal metamorphism on its parent body.

In previous work, Thomas et al. (1993b) analyzed $\sim$20 individual, small-sized IDPs, placed them into three groups based on their mineralogy, and speculated on sources for these particles. They suggested that the anhydrous pyroxene-dominated, C-rich IDPs originated from cometary rather than asteroidal sources because of their high bulk carbon abundance and the fine-grained pyroxene which are unlike any from chondrite matrix. They also suggested that the low-carbon, olivine-dominated anhydrous IDPs may be derived from anhydrous asteroids. In the present study, we have found both types of IDP material, those that are pyroxene-dominated and rich in carbon and those that are olivine-dominated and carbon poor, existing in one cluster particle. Are previous implications for IDP sources now incorrect? The prior study of small-sized IDPs provides a wealth of information on individual fragments, but without additional information to constrain entry velocities (e.g., noble gas measurements), identification of source parent bodies can be ambiguous (e.g., asteroidal or cometary). However, cluster particles present a unique opportunity to study inter-fragment relationships that can only be determined as we examine larger-sized IDPs.

CONCLUSIONS

1) Cluster L2008#5 displays a remarkable chemical and mineralogical heterogeneity on a size scale of the individual fragments which we analyzed (10–15 μm). The mineralogy and chemistry of the individual fragments span a wide range of previously analyzed anhydrous particles.
2) Despite this remarkable heterogeneity, there is strong evidence that nearly all of the analyzed fragments were originally part of the same $\sim$50 μm diameter cluster in space.
3) The low Earth-encounter velocity estimated for this particle (<14 km/s) is consistent with origin from an object in an asteroidal orbit.
4) This cluster is essentially a heterogeneous breccia made up of materials having different histories which were physically combined either in the early nebula or in the regolith of a parent body. We infer that the source region of this asteroid is a complex mixture of fragments and clasts from diverse sources having diverse histories; the resulting breccia represented by cluster L2008#5 has provided us with a rich sampling of many different products.
5) Heating during atmospheric entry has occurred and is quite variable, showing that thermal equilibrium was not attained. However, these heating effects can be unraveled using previously documented characteristics such as the formation of magnetite rims, helium measurements, and depletion of zinc.
6) These results on cluster L2008#5 provide an important cautionary note for attempts to interpret individual 10–15 μm IDPs as representative of parent bodies.

Acknowledgments—Constructive reviews of this manuscript were provided by John Bradley, two anonymous reviewers, and Sue Wentworth. This work was supported in part by NASA RTOPs 152-17-40-23 and 199-52-11-02.

Editorial handling: G. Crozaz

[§] These calculations were done using measurements of particle surface densities of small area collectors from Zolensky and MacKinnon (1985). Surface density measurements may be different on large area collectors but have not yet been determined.

REFERENCES

Adams N. G. and Smith D. (1981) $^{14}N/^{15}N$ Isotope fractionation in the reaction $N_2H^+ + N_2$: Interstellar significance. *Astrophys. J. Lett.* **247,** L123.

Anders E. and Grevesse N. (1989) Abundance of the elements: Meteoritic and solar. *Geochim. Cosmochim. Acta* **53,** 197–214.

Ash R. D., Morse A. D., and Pillinger C. T. (1993) The survival of presolar organic material in CR chondrites? *Meteoritics* **28,** 318–319 (abstr.).

Black D. C. (1972) On the origins of trapped helium, neon, and argon isotopic variations in meteorites-II. Carbonaceous meteorites. *Geochim. Cosmochim. Acta* **36,** 377–394.

Bradley J. P. (1994a) Nanometer-scale mineralogy and petrography of anhydrous interplanetary dust particles. *Geochim. Cosmochim. Acta* **58,** 2123–2134.

Bradley J. P. (1994b) Chemically anomalous, preaccretionally irradiated grains in interplanetary dust from comets. *Science* **265,** 925–929.

Bradley J. P. and Brownlee D. E. (1988) Analysis of chondritic interplanetary dust thin sections. *Geochim. Cosmochim. Acta* **52,** 899–900.

Bradley J. P., Brownlee D. E., and Keller L. P. (1994) Reflectance spectroscopy of individual interplanetary dust particles. *Lunar Planet. Sci.* **25,** 159–160 (abstr.).

Brownlee D. E., Joswiak D. J., and Love S. G. (1993) Identification of cometary and asteroidal particles in stratospheric IDP collections. *Lunar Planet. Sci.* **24,** 205–206 (abstr.).

Brownlee D. E., Joswiak D. J., Schlutter D. J., Bradley J. P., and Love S. G. (1995) Identification of individual cometary IDPs by thermally stepped He release. *Lunar Planet. Sci.* **26,** (in press). (abstr.)

Clemett S. J., Maechling C. R., and Zare R. N. (1992) Analysis of polycyclic aromatic hydrocarbons in seventeen ordinary and carbonaceous chondrites. *Lunar Planet. Sci.* **23,** 233–234 (abstr.).

Clemett S. J., Maechling C. R., Zare R. N., Swan P. D., and Walker R. M. (1993) Identification of complex aromatic molecules in individual interplanetary dust particles. *Science* **262**, 721–725.

Cronin J. R., Pizzarello S., Epstein S., and Krishnamurthy R. V. (1993) Molecular and isotopic analyses of the hydroxy acids, dicarboxylic acids, and hydrooxydicarboxylic acids of the Murchison meteorites. *Geochim. Cosmochim. Acta* **57**, 4745–4752.

Flynn G. J. (1989) Atmospheric entry heating: A criterion to distinguish between asteroidal and cometary sources of interplanetary dust particles. *Icarus* **77**, 287–310.

Flynn G. J. (1990) The near-Earth enhancement of asteroidal over cometary dust. *Proc. 20th Lunar Planet. Sci. Conf.*, 363–371.

Flynn G. J. (1994) Changes to IDP composition and mineralogy by terrestrial encounters. In *Analysis of Interplanetary Dust* (ed. M. E. Zolensky et al.); *AIP Conference Proceedings*, pp. 127–143.

Flynn G. J. (1995) Thermal gradients in interplanetary dust particles: The effect of an endothermic phase transition. *Lunar Planet. Sci.* **26**, (in press) (abstr.).

Flynn G. J. and Sutton S. R. (1990) Evidence for a bimodal distribution of cosmic dust densities. *Lunar Planet. Sci.* **21**, 375–376 (abstr.).

Flynn G. J. and Sutton S. R. (1991) Chemical characterization of seven large area collector particles by SXRF. *Proc. 21st Lunar Planet. Sci. Conf.*, 549–556.

Flynn G. J., Sutton S. R., Thomas K. L., Keller L. P., and Klöck W. (1992) Zn depletions and atmospheric entry heating in stratospheric cosmic dust particles. *Lunar Planet. Sci.* **23**, 375–376 (abstr.).

Flynn G. J., Sutton S. R., Bajt S., Klöck W., Thomas K. L., and Keller L. P. (1993) The volatile content of anhydrous interplanetary dust. *Meteoritics* **28**, 349–350 (abstr.).

Flynn G. J., Sutton S. R., Bajt S., Klöck W., Thomas K. L., and Keller L. P. (1994) Hydrated interplanetary dust particles: Element abundances, mineralogies, and possible relationships to anhydrous IDPs. *Lunar Planet. Sci.* **25**, 381–382 (abstr.).

Geiss J. and Reeves H. (1981) Deuterium in the solar system. *Astron. Astrophys.* **93**, 189–199.

Greinke R. A. and Lewis I. C. (1984) Carbonization of naphthalene and dimethylnapthalene. *Carbon* **22**, 305–314.

Grün E., Zook H. A., Fechtig H., and Giese R. H. (1985) Collisional balance of the meteoritic complex. *Icarus* **62**, 244–273.

Hiroi T., Pieters C. M., and Zolensky M. E. (1993) Comparison of reflectance spectra of C asteroids and unique C chondrites Y86720, Y82162, and B7904. *Lunar Planet. Sci.* **24**, 659–660 (abstr.).

Huss G. R., Keil K., and Taylor G. J. (1981) The matrices of unequilibrated ordinary chondrites: Implication for the origin and history of chondrites. *Geochim. Cosmochim. Acta* **45**, 33–51.

Jessberger E. K., Christoforisis A., and Kissel J. (1988) Aspects of the major element composition of Halley dust. *Nature* **332**, 691–695.

Keller L. P., Thomas K. L., and McKay D. S. (1992) Thermal processing of cosmic dust: atmospheric heating and parent body metamorphism. *Lunar Planet. Sci.* **23**, 675–676 (abstr.).

Kerridge J. F. (1985) Carbon, hydrogen, and nitrogen in carbonaceous chondrites: Abundances and isotopic compositions in bulk samples. *Geochim. Cosmochim. Acta* **49**, 1707–1714.

Klöck W., Thomas K. L., McKay D. S., and Palme H. (1989) Unusual olivine and pyroxene composition in interplanetary dust and unequilibrated ordinary chondrites. *Nature* **339**, 26–128.

Klöck W., Thomas K. L., McKay D. S., and Zolensky M. E. (1990) Olivine compositions in anhydrous and hydrated IDPs compared to olivines in matrices of primitive metorites. *Lunar Planet. Sci.* **21**, 637–638 (abstr.).

Kovalenko L. J., Maechling C. R., Clemett S. J., Phillopoz J. M., Zare R. N., and Alexander C. M. O'D., (1992) Microscopic organic analysis using two-step laser mass spectrometry: Application to meteoritic acid residues. *Anal. Chem.* **64**, 682–690.

Krishnamurthy R. V., Epstein S., Cronin J. R., Pizzarello S., and Yeun G. U. (1992) Isotopic and molecular analyses of hydrocarbons and monocarboxylic acids of the Murchinson meteorite. *Geochim. Cosmochim. Acta* **56**, 4045–4058.

Lewis I. C. (1979) Thermal polymerization of aromatic hydrocarbons. *Carbon* **18**, 191–196.

Love S. G. and Brownlee D. E. (1991) Heating and thermal transformation of micrometeorids entering the Earth's atmosphere. *Icarus* **89**, 26–43.

Love S. G. and Brownlee D. E. (1993) A direct measurement of the terrestial mass accretion rate of cosmic dust. *Science* **262**, 550–553.

Love S. G. and Brownlee D. E. (1994) Peak atmospheric entry temperatures of micrometeorites. *Meteoritics* **29**, 69–70.

Love S. G., Joswiak D. J., and Brownlee D. E. (1994) Densities of stratospheric micrometeorites. *Icarus* **111**, 227–236.

McKay D. S., Swindle T. D., and Greenberg R. (1989) Asteroidal regoliths: What we do not know. In *Asteroids II* (ed. R. P. Binzel et al.), pp. 617–642. Univ. Arizona Press.

McKeegan K. D., Walker R. M., and Zinner E. (1985) Ion microprobe isotopic measurements of individual interplanetary dust particles. *Geochim. Cosmochim. Acta* **49**, 1971–1987.

McKeegan K. D., Swan P., Walker R. M., Wopenka B., and Zinner E. (1987) Hydrogen isotopic variations in interplanetary dust particles. *Lunar Planet. Sci.* **18**, 627–628 (abstr.).

McNaughton N. J., Borthwick J., Fallick A. E., and Pillinger C. T. (1981) Deuterium/hydrogen ratios in unequilibrated ordinary chondrites. *Nature* **294**, 639–641.

McSween H. Y., Jr., and Richardson S. M. (1977) The composition of carbonaceous chondrite matrix. *Geochim. Cosmochim. Acta* **41**, 1145–1161.

Nier A. O. and Schlutter D. J. (1992) Extraction of helium from individual interplanetary dust particle by step-heating. *Meteoritics* **27**, 166–173.

Nier A. O. and Schlutter D. J. (1993) The thermal history of interplanetary dust particles collected in the Earth's stratosphere. *Meteoritics* **25**, 675–681.

Pizzarello S., Krishnamurthy R. V., Epstein S., and Cronin J. R. (1991) Isotopic analyses of amino acids from the Murchinson meteorite. *Geochim. Cosmochim. Acta* **55**, 905–910.

Rietmeijer F. J. M. (1993) Size distributions in two porous chondritic micrometeorites. *Earth Planet. Sci. Lett.* **117**, 609–617.

Schramm L. S., Brownlee D. E., and Wheelock M. M. (1989) Major element composition of stratospheric micrometeorites. *Meteoritics* **24**, 99–112.

Schultz L. and Kruse H. (1989) Helium, neon, and argon in meteorites-a data compilation. *Meteoritics* **24**, 155–172.

Stadermann F. J., Walker R. M., and Zinner E. (1989) Ion microprobe measurements of nitrogen and carbon isotopic variations in individual IDPs. *Meteoritics* **24**, 327 (abstr.).

Sutton S. R. and Flynn G. J. (1988) Stratospheric particles: Synchrotron x-ray fluorescence determination of trace element contents. *Proc. 18th Lunar Planet. Sci. Conf.*, 607–614.

Tedesco E. F. (1989) Asteroid magnitudes. UBV colors, and IRAS albedos and diameters. In *Asteroids II* (ed. R. P. Binzel et al.), pp. 1090–1138. Univ. Arizona Press.

Thomas K. L., Keller L. P., Flynn G. J., Sutton S. R., Takatori K., and McKay D. S. (1992) Bulk compositions, mineralogy, and trace element abundances of six interplanetary dust particles. *Lunar Planet. Sci.* **23**, 1427–1428 (abstr.).

Thomas K. L., Klöck W., Keller L. P., Blanford G. E., and McKay D. S. (1993a) Analysis of fragments from cluster particles: Carbon abundances, bulk chemistry, and mineralogy. *Meteoritics* **28**, 448–449 (abstr.).

Thomas K. L., Blanford G. E., Keller L. P., Klöck W., and McKay D. S. (1993b) Carbon abundance and silicate mineralogy of anhydrous interplanetary dust particles. *Geochim. Cosmochim. Acta* **57**, 1551–1566.

Thomas K. L., Keller L. P., Blanford G. E., and McKay D. S. (1994) Quantitative analyses of carbon in anhydrous and hydrated interplanetary dust particles. In *Analysis of Interplanetary Dust* (ed. M. E. Zolensky et al.); *AIP Conference Proceedings*, pp. 165–172.

Zellner B., Tholen D. J., and Tedesco E. F. (1985) The eight-color asteroid survey: results for 589 minor planets. *Icarus* **61**, 355–416.

Zenobi R. and Zare R. N. (1991) Two-step laser spectrometry. In *Advances in Multiphoton Processes and Spectroscopy* (ed. S. H. Lin), Vol. 7, pp. 1–167. World Scientific Publishing.

Zolensky M. E. and MacKinnon I. D. R. (1985) Accurate stratospheric particle size distributions from a flat-plate collection surface. *J. Geophys. Res.* **90**, 5801–5808.